Experimental study of gas-fluidized granular flows with implications for pyroclastic flow emplacement

Olivier Roche, M. Gilbertson, J. Phillips, R. Sparks

Experimental study of gas-fluidized granular flows with implications for pyroclastic flow emplacement

O. Roche[1]

UMR Magmas et Volcans, Institut de Recherche pour le Développement, Université Blaise Pascal, Clermont-Ferrand, France

M. A. Gilbertson

Department of Mechanical Engineering, Centre for Environmental and Geophysical Flows, University of Bristol, Bristol, UK

J. C. Phillips and R. S. J. Sparks

Department of Earth Sciences, Center for Environmental and Geophysical Flows, University of Bristol, Bristol, UK

Received 28 November 2003; revised 22 July 2004; accepted 29 July 2004; published 5 October 2004.

[1] Experiments have been carried out on initially gas-aerated and gas-fluidized granular flows propagating into a horizontal channel. After lateral acceleration following release of the originally fluidized bed, two contrasting flow behaviors were observed, which reflected the degree of initial fluidization and the grain size. Initial fluidization disrupts the interparticle contact network, which controls internal friction of the static bed. The flow regime then depends on the timescale needed to reestablish a strong contact network, and this time increases as the grain size decreases. Initially aerated and fluidized flows of coarse particles ($>\approx$100 μm) and initially aerated flows of fine particles ($<\approx$100 μm) behave as their nonfluidized counterparts and they propagate as a wedge, with decelerating velocities so that the front position increases as the $\sim$0.8 power of time. In contrast, initially fluidized flows of fine particles propagate for most of their duration at constant thickness and frontal velocity in a similar fashion to the slumping regime of buoyancy-driven gravity currents of Newtonian fluids. We have determined a Froude number *Fr* for such flows of $\approx$2.6 consistent with published data from experimental and theoretical investigations on inviscid fluids. This implies that internal particle friction can be neglected in describing the dynamics of initially fluidized, concentrated fine granular flows. However, all flows are characterized by a short, final stopping phase whose timescale gives an estimate of the kinetics required to reestablish a strong contact network and form a static deposit. These results suggest that fines-rich pyroclastic flows may propagate as inviscid fluids for most of their emplacement. *INDEX TERMS:* 8414 Volcanology: Eruption mechanisms; 8499 Volcanology: General or miscellaneous; 8429 Volcanology: Lava rheology and morphology; *KEYWORDS:* volcanology, explosive volcanism, pyroclastic flows, fluidization, experiments, granular flows, fluid gravity currents

Citation: Roche, O., M. A. Gilbertson, J. C. Phillips, and R. S. J. Sparks (2004), Experimental study of gas-fluidized granular flows with implications for pyroclastic flow emplacement, *J. Geophys. Res.*, *109*, B10201, doi:10.1029/2003JB002916.

1. Introduction

[2] Granular flows are common phenomena in natural and man-made processes, and understanding their dynamics is critical for hazard assessment and industrial optimization. Many studies have focused on dry granular flows of cohesionless particles for which the role of the interstitial fluid phase is negligible [e.g., *Savage*, 1984; *Campbell*, 1990; *Goldhirsch*, 2003]. Many of these investigations are concerned with steady flows down a rough incline, at an angle greater than that of the angle of repose of the material used. Early works [e.g., *Savage*, 1984; *Savage and Hutter*, 1989] developed continuum models with the granular mass treated as a frictional Coulomb material with a Coulomb-like basal friction law. Depth-averaged equations of motion for mass and momentum can be derived to give the evolution of the flow geometry and velocity, and are analogous to the nonlinear shallow-water wave equations. These models assume rate independence for bed friction angle and a constant velocity profile. The physical similarity between the interaction of grains in granular flows at relatively high shear rate and the interaction of molecules described by the kinetic theory of gases led several authors to derive continuum equations from microscopic models of individual particles interactions [*Johnson and Jackson*,

[1]Also at Department of Earth Sciences, Centre for Environmental and Geophysical Flows, University of Bristol, Bristol, UK.

0148-0227/04/2003JB002916$09.00

1987; *Campbell*, 1990; *Goldhirsch*, 2003]. This is known as the kinetic grain theory and these studies developed the concept of granular temperature, which is a measure of the kinetic energy of random motions of the particles. Frictional effects can be combined with kinetic theory by assuming that the total stress transmitted by the particles is the sum of the frictional and collisional contributions calculated independently. *Johnson et al.* [1990] found that collision is the principal mechanism near the free surface while frictional effects become dominant at depth. *Pouliquen* [1999a] developed scaling laws by studying the variation of the mean velocity with the plane inclination and with the thickness of the granular layer. He measured the minimum flow thickness necessary to observe a steady uniform flow at a given inclination, and developed an empirical description of flows in terms of a dynamic friction coefficient. When this empirical law was included in the depth averaged momentum equation [e.g., *Savage and Hutter*, 1989], the front profile of experimental flows was successfully reproduced [*Pouliquen*, 1999b]. However, the importance of internal friction in unsteady granular flows has been recently questioned by experiments on flows generated from slumping piles and propagating on a horizontal surface [*Lube et al.*, 2004]. These flows can be quantitatively described independently of any friction coefficient, apart for the last instant of emplacement when they stop abruptly. Numerical modeling by *Mangeney-Castelnau et al.* [2003] of a similar configuration using shallow water (Saint Venant) equations also suggested that friction is important only during stopping of the granular mass, when the driving forces are comparable to the Coulomb threshold. A recent review also emphasized that friction may not be important in fast dense flows within which particles are highly agitated and which behave in a fluid-like manner [*Groupement de Recherche Milieux Divisés* (*G. D. R. Midi*), 2004].

[3] Few studies have taken into account the role of an interstitial gaseous phase to promote fluidization of the dense granular medium and reduce internal friction. *Ishida et al.* [1980] carried out experiments on granular flows over an inclined surface through which gas was flowing. When the gas flow velocity was below that which can support the particles' weight (U_{mf}, see section 2) and the slope was equal to the angle of repose, an immature sliding flow formed consisting of a stationary basal layer with an upper flow transitional between a quasistatic and a fully developed state. Sliding flows with no static region at the base occurred at higher gas flow rates. In contrast, when the gas flow velocity exceeded U_{mf}, a flow could occur even when the slope was significantly smaller than the angle of repose. This situation was investigated theoretically by *Nott and Jackson* [1992] at a gas flow velocity less than U_{mf}. They showed that compared to nonfluidized flows, the magnitudes of the stresses are reduced, but a higher proportion of the stresses are generated by collision rather than by friction. In contrast, *Eames and Gilbertson* [2000] investigated similar gas particle flows but on a horizontal surface and showed that interparticle friction dominates and collisional effects are negligible. When the gas flow was increased, the upper slope of the flow decreased by adjustment through bulk movement or avalanching; these observations implied reduction of internal friction due to air drag with increasing support of the weight of the particles. They developed a mathematical model that successfully reproduced their experimental results on channeled and axisymmetric flows. The model, based on depth-averaged equations, included the momentum exchange between gas and particles and described the size and shape of the flow with no adjustable parameters. *Takahashi and Tsujimoto* [2000] carried out experiments on fluidized flows in a two-dimensional channel inclined at angles of 5.5° to 24°. The fluidized mixture was generated by mixing sodium hydrogen carbonate into heated fine sand, which generated gases with an interstitial fluid velocity sufficiently large to support the particles fully. Flows were generated by pouring the mixture into the flume. The flows consisted of a lower, dense layer and an upper, thinner and dilute layer.

[4] Some geophysical flows are examples of gas-fluidized concentrated granular mixtures. While recognizing their complexities, geophysical flows may share many of the features of the monodisperse granular flow systems that have been so widely studied in the laboratory. Geophysical flows include pyroclastic density currents, which consist of hot mixtures of volcanic gas and particles and represent an important natural hazard. They encompass a range of phenomena, from dense gas-fluidized pyroclastic flows to dilute turbulent flows dominated by the gaseous phase [*Druitt*, 1998; *Branney and Kokelaar*, 2002]. This study focuses on dense pyroclastic flows that generate ignimbrites [*Sparks*, 1976; *Wilson*, 1980, 1984]. These flows are generated from the gravitational collapse of lava domes and during explosive eruptions from collapsing fountains, and have typical volumes in the range of 10^{-3}–10^{1} km^3 [*Druitt*, 1998; *Branney and Kokelaar*, 2002]. The fluidizing gas can be generated at the vent as well as being ingested at the flow front or released by the particles [*Sparks*, 1978; *Wilson*, 1984]. Pyroclastic flows can propagate over distances of several kilometers to tens of kilometers on slopes of only a few degrees [*Hoblitt*, 1986; *Cole et al.*, 2002]. Their emplacement mechanism is still debated and information is required to better constrain their dynamical behavior in order, for instance, to predict their propagation velocity and run-out [*Druitt*, 1998; *Branney and Kokelaar*, 2002].

[5] In this paper we address the effect of the initial state of a bed of particles on the subsequent motion of a particle flow over a horizontal surface in a confined channel of constant width. The run-out of a granular flow can be greatly increased by continuous fluidization [*Eames and Gilbertson*, 2000]. In addition, the behavior of such fluidized flows may depend on the particle size due to interparticle forces. Even when interparticle forces are weak, they can greatly retard the motion of a current and cause it to move intermittently owing to its small height [*Gilbertson and Eames*, 2003]. However, the dynamics of flows that are fluidized only prior to their release are poorly understood. We have investigated the role of the grain size of the particles and the degree of initial fluidization for a range of initial bed heights on the run-out of flows. In particular, we show that, under certain initial conditions, initially gas-fluidized granular

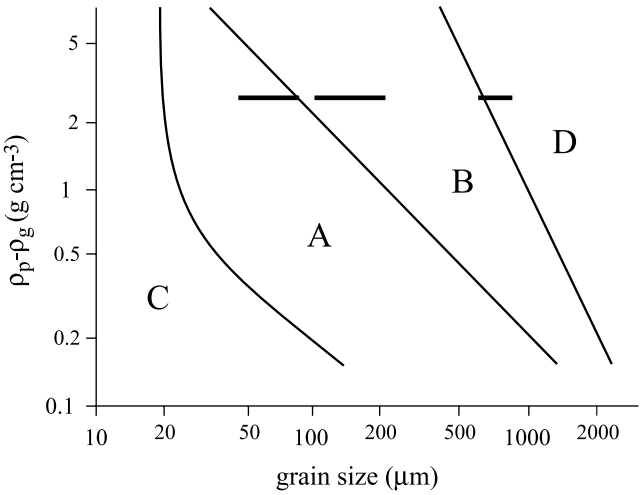

Figure 1. *Geldart*'s [1973] classification for gas-fluidized granular beds. Here ρ_p and ρ_g are the particles and gas densities, respectively. The thick horizontal lines are the grain size ranges of the particles used in our experiments.

flows can behave in a similar way to buoyancy-driven gravity currents of a Newtonian fluid. This paper extends the results of a preliminary study by *Roche et al.* [2002].

2. Principles of Gas Fluidization

[6] Gas-fluidization has many engineering applications (see *Rhodes* [1998] for review). Gas flowing vertically through a granular bed exerts a drag force on the particles that increases with the gas flow rate. The pressure drop across the bed increases with the gas velocity as can be described using the semiempirical Ergun equation:

$$\frac{\Delta p}{h} = \frac{150(1-\varepsilon)^2 \mu_g U_g}{\varepsilon^3 d_p^2} + \frac{1.75(1-\varepsilon)\rho_g U_g^2}{\varepsilon^3 d_p}, \qquad (1)$$

where $\Delta p/h$ is the pressure drop across the bed of height h, ε is the bed porosity, μ_g is the gas dynamic viscosity, U_g is the superficial gas velocity (defined as the gas flow rate divided by the bed cross sectional area), d_p is the surface volume particle diameter, and ρ_g is the gas density [*Rhodes*, 1998]. The first and second terms of the right-hand part of equation 1 are respectively the contributions of viscosity and inertia to drag. If U_g is increased, the pressure drop increases and the weight of the bed is increasingly supported. At this stage, the bed is static and commonly termed aerated. The internal friction of an aerated granular pile is progressively reduced as the gas flow rate increases which is reflected in a reduction of the slope angle of the pile [*Eames and Gilbertson*, 2000]. The total weight of the bed is supported by the gas flux at the minimum fluidization velocity U_{mf}, so that

$$\frac{\Delta p}{h} = \left(1-\varepsilon_{mf}\right)\left(\rho_p - \rho_g\right)g, \qquad (2)$$

where ε_{mf} is the voidage at the point of minimum fluidization, ρ_p is the density of the particles, and g is the acceleration due to gravity [*Rhodes*, 1998]. A fundamental property of fluidized granular media is that internal friction is very much reduced and they flow in a fluid-like manner.

[7] The behavior of gas-fluidized beds at room temperature and pressure was classified empirically by *Geldart* [1973], based on the grain size of the particles and the density difference between the particles and the gas (Figure 1). Very fine powders (group C), for which cohesion dominates, cannot readily be fluidized and vertical and horizontal channels commonly form in the bed, which is partially lifted up as a plug. Fine particles of group A can be homogeneously fluidized until gas bubbles form at a second critical velocity, the minimum bubbling velocity, $U_{mb} > U_{mf}$. Before bubble formation ($U_{mf} < U_g < U_{mb}$) the bed expands linearly as U_g increases, to a maximum at U_{mb}. When $U_g > U_{mb}$, the dense phase voidage remains approximately constant but the bulk bed expansion increases as more bubbles form with increasing flow rate. For coarse particles of groups B and D, gas bubbles form at U_{mf} and fluidization is heterogeneous. The dense phase expansion is very limited (group B) or almost absent (group D). For group B, the bubbles are typically isolated, while for group D the particles are so coarse that there can be open gas flow through interconnected bubbles. Bubble size increases with the gas velocity for both groups and the bulk bed expansion may be significantly larger than the dense phase expansion (e.g., Table 1).

[8] If the air supply is stopped, the bed defluidizes and this phenomenon is relevant for some of the experiments described here. *Geldart and Wong* [1985] studied the collapse of an initially expanded fluidized bed (at $U_g > U_{mf}$) of group A particles. They showed that after rapid evacuation of bubbles, the collapse occurs at a constant deaeration rate (U_{de}), which is the velocity at which the top of the bed moves downward. Our measurements using different types of particles showed that U_{de} increases with grain size and is typically 2 orders of magnitude less than the terminal fall velocity of individual particles. For group B particles, U_{de} could be related to bubble evacuation only, whereas for group D particles, U_{de} cannot be defined, as there is no dense phase expansion (Table 1).

3. Experimental Apparatus, Material, and Procedure

[9] The experimental apparatus is shown in Figure 2. The granular material is fluidized in a reservoir by introducing an air flux through a 10 mm thick porous plate (Porvair Vyon D). The bed is fluidized to various degrees with

Table 1. Properties of the Beds of Particles Used in Experiments

	Group		
	A	B	D
Grain size range, μm	45–90	106–212	600–800
Bulk density, kg m^{-3}	1492	1467	1450
Angle of repose φ, deg	28.5	24.5	24
Porosity ε	0.40	0.41	0.42
Minimum fluidization velocity U_{mf}, cm s^{-1}	0.83	2.16	27.0
Deaeration rate U_{de}, cm s^{-1}	0.62	1.35	...
Maximum dense phase expansion, %	7–8	~2–3	~0
Maximum bulk bed expansion, %	10–12	~35	~40

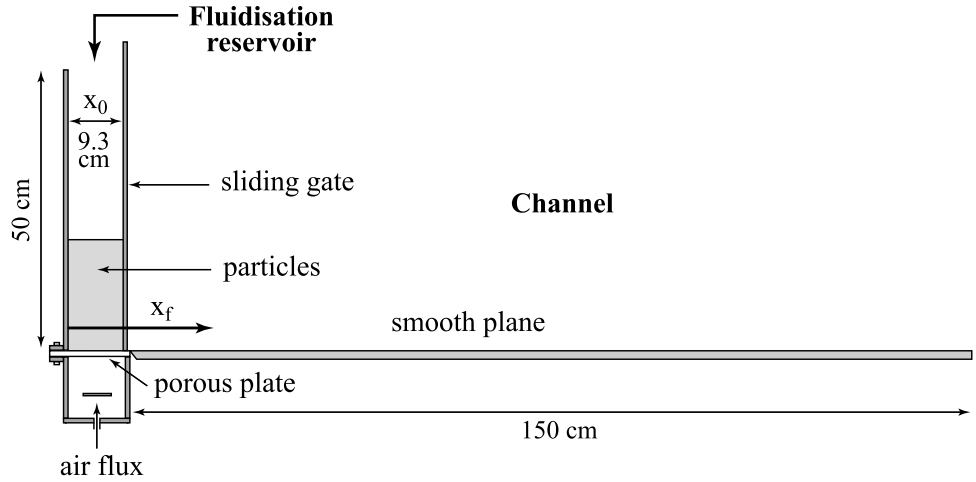

Figure 2. Experimental apparatus. The fluidization reservoir (length x_0) and the channel have similar constant widths of 8 cm. One side of the channel is made of a Plexiglas plate for video recordings. Flow run-out (x_f) is measured from the backwall of the reservoir.

U_g/U_{mf} ranging from 0 to 25, and it is referred hereafter as nonfluidized ($U_g/U_{mf} = 0$), aerated ($0 < U_g/U_{mf} < 1$), or fluidized ($U_g/U_{mf} \geq 1$). At the highest degrees of fluidization, the bed is vigorously agitated and the bulk bed expansion is up to about $\approx$1.1–1.4 times the initial bed thickness (Figure 3). Beds of group A particles progressively expand as U_g approaches U_{mb} and the maximum dense phase expansion is $\approx$7–8%. The fluidized bed is macroscopically homogenous at this stage. Bubbles form at $U_g/U_{mf} > \sim 2$, with a maximum bulk bed expansion of $\approx$12–13% at $U_g/U_{mf} = 25$. Bulk bed expansion for group B particles increases until $U_g/U_{mf} \approx 10$ and then stabilizes at $\approx$35% for higher velocities, whereas for group D particles expansion increases until $U_g/U_{mf} \approx 2.5$ and then stabilizes at $\approx$40%. Beds are highly agitated at high velocities. Experiments for group D particles at $U_g/U_{mf} > 2.5$ were not studied in detail because the bubbles had a size comparable to that of the reservoir. The presence of these large bubbles dominates the subsequent flow, causing it to pulsate and have nonreproducible velocity, thickness, and run-out.

[10] The bed is released into a channel of uniform width by means of a sliding gate, thus creating a flow that propagates along a horizontal, smooth surface. No air flux is provided from the base of the channel and the flow defluidizes as it propagates. The particles used are nearly spherical glass beads (ballotini) of density $\rho_p = 2500$ kg m^{-3} with a small grain size range (Table 1). For a range of initial bed heights in the reservoir, we investigated the influence of the degree of initial fluidization of the bed (U_g/U_{mf}) and of the grain size (i.e., Geldart group) of the particles on flow dynamics.

[11] For each experiment, we measured the length of the deposit from the backwall of the fluidization reservoir (x_f, hereinafter referred to as the flow run-out, Figure 2). Most of the deposits viewed from above had a flat front perpendicular to the sides of the channel. In some cases the front was slightly curved or slanted on one side by 1–2 cm and we then measured a mean flow run-out with a precision of 0.5 cm. Repetition of experiments showed a maximum variation in the flow run-out of 1 cm and 3 cm for smaller ($x_f \sim 30$ cm) and longer ($x_f \sim 110$ cm) flows, respectively. We measured the thickness of the deposits at intervals of 2–5 cm with a precision of 0.5 mm. Frames captured from video recordings through one side of the channel made of

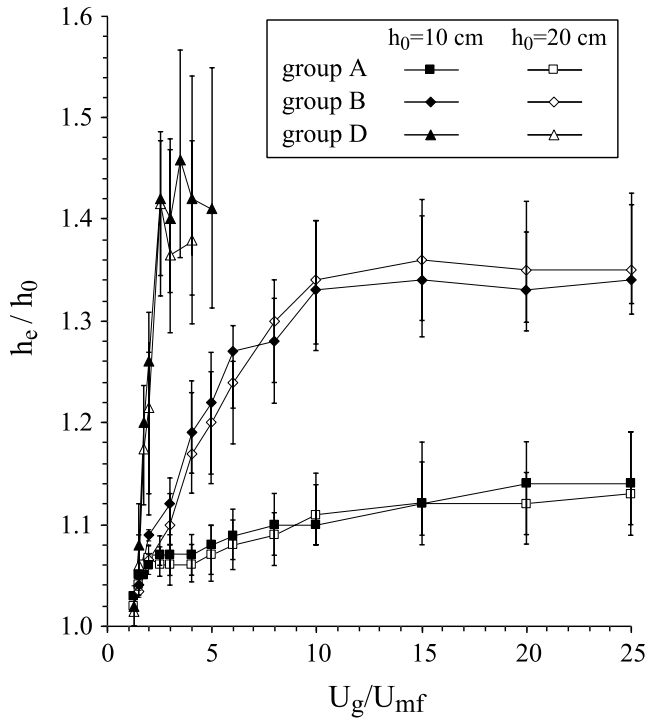

Figure 3. Expansion of the bed in the reservoir as a function of the degree of fluidization (U_g/U_{mf}), h_e and h_0 are the height of the expanded and nonexpanded beds, respectively. Mean values and range of bed height variations are shown for bubbling beds. Bubbles form at $U_g/U_{mf} = 1$ for groups B and D particles and at $U_g/U_{mf} \approx 2$ for group A particles. Experiments at $U_g/U_{mf} > 2.5$ were not studied in detail for group D particles.

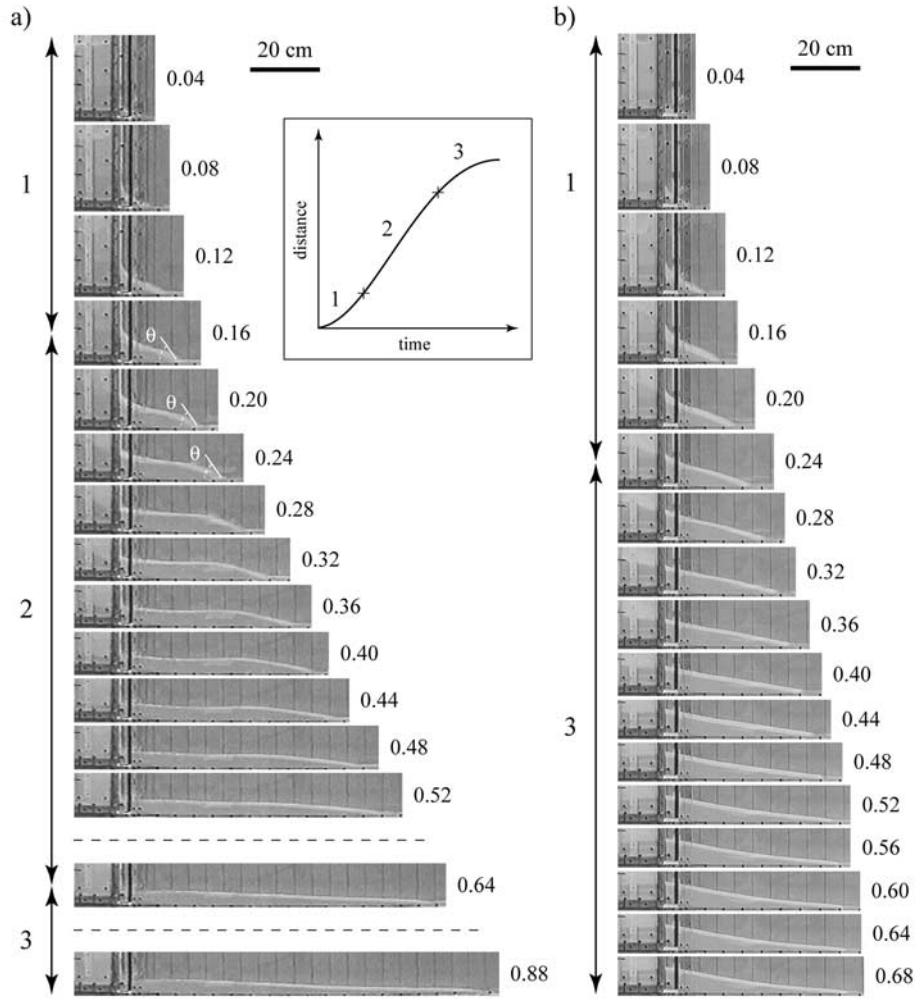

Figure 4. Emplacement of flows of particles of groups (a) A and (b) B generated from incipiently, nonexpanded fluidized beds ($U_g = U_{mf}$) of height $h_0 = 20$ cm. Numbers correspond to time in 1/100 s and last pictures are the final deposits. The thin vertical black lines in the channel are at 5 cm intervals. The slope angle to the horizontal of the flow front is $\Theta \sim 50°–60°$ for group A particles. Insert shows that flows occur in distinct phases: 1 (acceleration), 2 (constant velocity), 3 (deceleration), also shown for pictures on vertical arrows. Note that phase 2 is only present for group A particles.

plexiglass allowed detailed analysis of the flow kinematics, and the flow front position was recorded at intervals of 0.04 s. The flow front usually appeared blurred and we could only determine its position with a precision of 0.5 cm. The upper surface of the flow was sharply defined and we measured its thickness with a precision of 1 mm.

4. Experimental Results

4.1. Flow Emplacement

[12] The emplacement of two representative flows generated from fluidized beds is shown in Figure 4. Flow emplacement typically occurs in less than one second. For particles of group A (Figures 4a and 5), the flow passes through three phases. First, the flow emerges from the bottom of the bed and accelerates, and the front thickness rapidly decreases downstream ($0.04 < t < 0.16$ s). Second, the flow propagates at an approximately constant velocity ($0.16 < t < 0.64$ s). In the early stages of this phase the body of the flow has nearly constant thickness along its length. The slope of the flow front is initially $\approx 50°–60°$ and decreases with time. The main body of the flow remains constant in thickness until the bed height in the reservoir has decreased to the same thickness as the flow. Thereafter the flow acquires a wedge shape. This transition occurs at $0.40 < t < 0.44$ s. In some experiments, the thickness of the flow body is a few millimeters less than that of the head and of the tail. Third, the flow decelerates and stops ($0.64 < t < 0.88$ s). In contrast, flows generated from fluidized beds of particles of groups B (Figures 4b and 5) and D (Figure 5), and those generated from nonfluidized ($U_g = 0$) or aerated ($U_g < U_{mf}$) beds of any group of particles propagate as a wedge, accelerating and then decelerating with no intermediate constant-velocity phase. The run-out is much less than that of initially fluidized flows of group

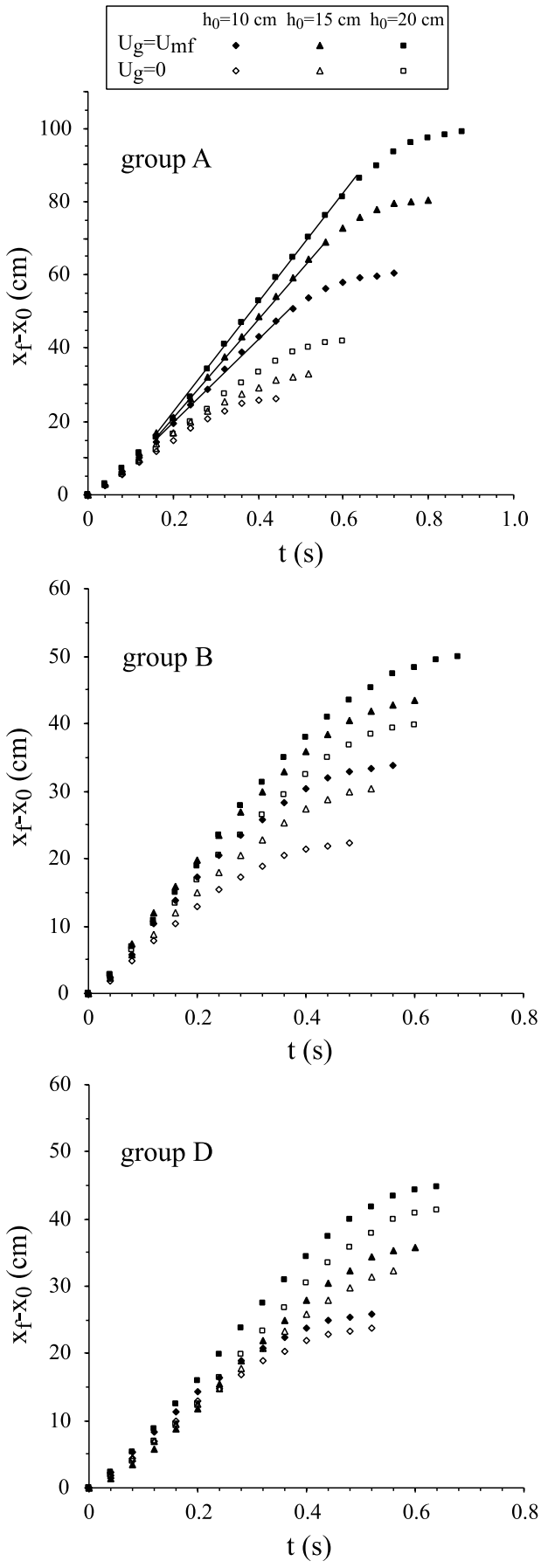

A particles with the same mass (Figures 4 and 5). Thickness does not decrease once a flow has come to rest, showing that it propagates as a highly concentrated dispersion.

4.2. Kinematic Data

[13] Kinematic data are presented in Figure 5 for flows generated from nonfluidized ($U_g = 0$) and initially fluidized ($U_g = U_{mf}$) beds. Initially fluidized flows propagate more rapidly than their nonfluidized analogs for a given initial bed height, and the velocity contrast increases as the grain size decreases: for group D particles the difference is small, but for group A particles initially fluidized flows travel about twice as far as their nonfluidized counterparts. All flows show acceleration and deceleration stages. Initially fluidized flows of group A particles also have an intermediate constant velocity phase and propagate at 0.9–1.6 m s^{-1} (Figure 5). For nonfluidized flows, the initial lateral acceleration is ≈0.3–0.4 g. For initially fluidized flows, the initial acceleration increases as the grain size decreases: it is 0.3–0.4 g for group D particles and so comparable to the nonfluidized cases, but it is 0.6–0.7 g for group B particles and 0.9–1 g for group A particles.

[14] For initially fluidized flows of group A particles, the acceleration and deceleration phases have constant durations of ≈0.16 s and ≈0.24 s, respectively, for bed heights h_0 of 10–20 cm (Figure 5). The acceleration and deceleration represents a decreasing proportion of the total flow duration as h_0 increases from 10 to 20 cm: from 22 to 18% for acceleration and from 33 to 27% for deceleration. The relative duration of the constant velocity phase thus increases as h_0 increases (from 45 to 55%). Experiments carried out at h_0 up to 30 cm reveal a slight increase in the acceleration phase duration, but confirm a constant timescale for the deceleration phase which represents only 23% of the whole flow duration at h_0 = 30 cm. Comparison with Figure 4 reveals that the phase of constant flow thickness ($0.16 < t < 0.44$ s), lasts for about two thirds of the constant velocity phase ($0.16 < t < 0.64$ s). This shows that though the flow is no longer fed from the reservoir and acquires a wedge shape, it still propagates at a constant velocity for some time ($0.44 < t <$ 0.64s).

[15] Figure 6 shows that the degree of initial fluidization, and hence bed expansion, has little influence on the emplacement of flows generated from fluidized beds for which $U_g/U_{mf} \geq 1$. Kinematic data are similar for initially fluidized flows of group A particles at U_g/U_{mf} of 1 (nonexpanded) to 20 (expanded, highly agitated). Similar behavior is observed for group B and D particles, except that

Figure 5. Kinematic data showing the flow front position from the reservoir gate ($x_f - x_0$) as a function of time (t). Flows were generated from nonfluidized ($U_g = 0$) and incipiently, nonexpanded fluidized beds ($U_g = U_{mf}$) of initial heights h_0 = 10–20 cm. Note the different scales. Initially fluidized flows of group A particles show a constant velocity phase (thin lines), which develops for an increasing part of the flow duration as h_0 increases. The thickness of these flows is constant for approximately the first two thirds of the duration of the constant velocity phase.

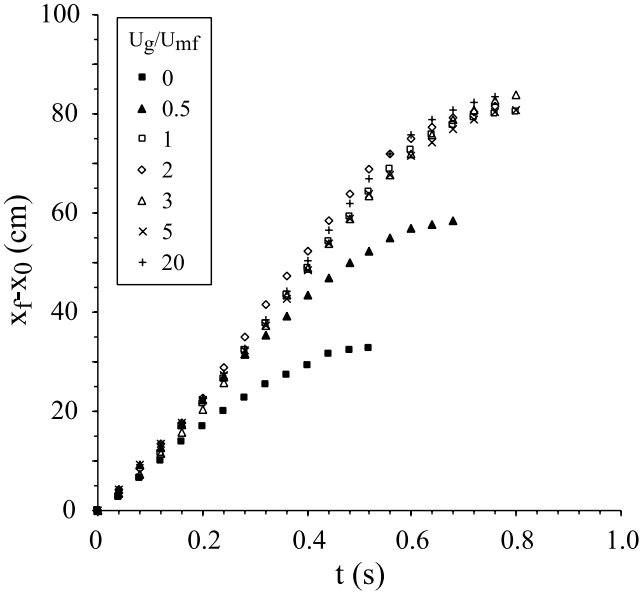

Figure 6. Kinematic data showing the flow front position from the reservoir gate ($x_f - x_0$) as a function of time (t), for flows of group A particles generated from beds of height h_0 = 15 cm at various degrees of initial fluidization (U_g/U_{mf}).

kinematic data become comparable only at $U_g/U_{mf} > 2–3$. Initially aerated flows ($U_g/U_{mf} = 0.5$) represent an intermediate case between nonfluidized and initially fluidized flows.

4.3. Flow Run-Out

[16] Figure 7 shows the run-out distances of flows generated from beds at various initial degrees of fluidization (U_g/U_{mf}). The run-out increases almost linearly as the bed is increasingly aerated for $0 < U_g/U_{mf} < 1$. When $U_g/U_{mf} > 1$ the run-out only depends weakly on the degree of initial fluidization. For group A particles, the run-out is maximum at $U_g/U_{mf} = 1.25$, then slightly decreases until $U_g/U_{mf} = 5–6$ and is roughly constant for $U_g/U_{mf} > 6$. Note that bubbles form in the bed at $U_g/U_{mf} \approx 2$. For groups B and D particles, the run-out distances continue to increase until $U_g/U_{mf} = 10$ and 2.5 respectively, which correspond to the highest bulk bed expansions (Figure 3). The run-out distances of initially aerated and fluidized flows also increase as the grain size decreases, and the contrast in run-out distances between group A and coarser particles is the highest at $U_g/U_{mf} = 1.25$.

[17] In order to make a valid comparison of fluidized and nonfluidized flows with the same mass of particles in the flow, a slight correction needs to be made for the differences in the mass involved in flow for experiments with the same bed height (Figure 7b). For a fluidized bed all the material is involved in the motion. In contrast, for the same bed height less material is involved for a nonfluidized bed because a static region of particles remains in the reservoir as a pile with a slope approximately equal to the angle of repose of the material forms. Consequently the mass of the flow is reduced compared to the fully fluidized case. For an aerated bed, the volume of static material left behind decreases as the system approaches incipient fluidization. On flow release, the slope of the pile can be assumed to be $\varphi_U = \varphi_0[1 - (U_g/U_{mf})]$, where φ_0 is the angle of repose of the nonfluidized material. The run-out, x_f, is plotted as a function of the estimated 2-D volume involved in motion, as measured by the difference between the total volume given by $h_0 x_0$ (where h_0 is the initial bed height and x_0 the reservoir length) and the static volume left behind in the reservoir as given by $0.5x_0^2 \tan \varphi_U$, and the relationship is linear. This allows comparison between the run-out of fully fluidized

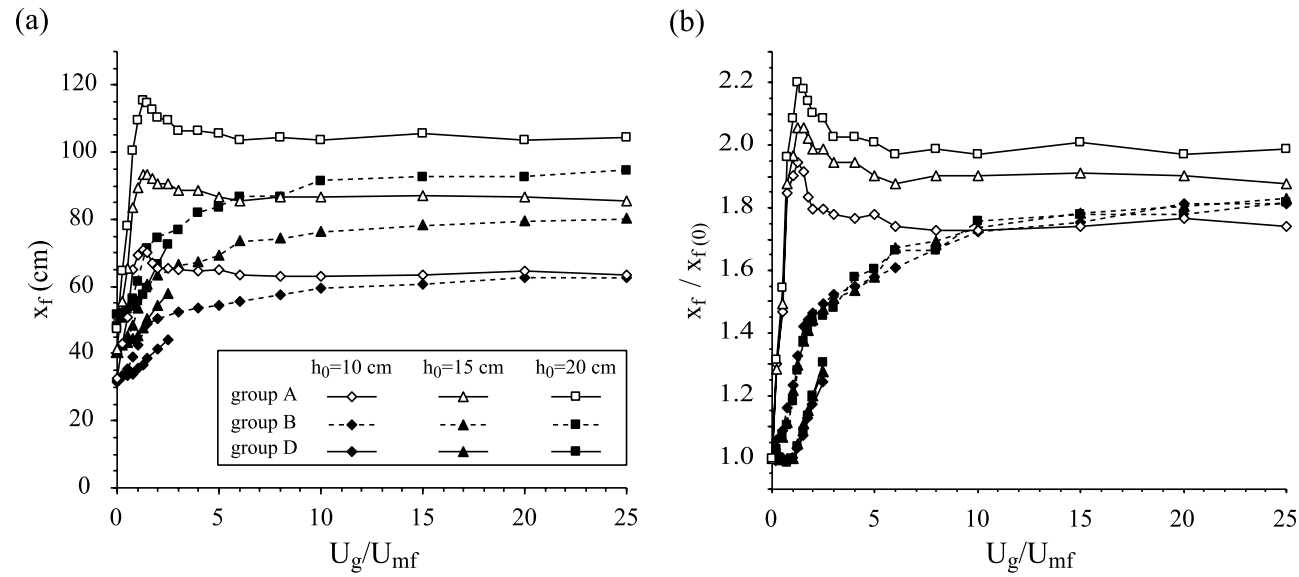

Figure 7. (a) Flow run-out (x_f) and (b) relative increase in flow run-out as a function of the degree of initial fluidization (U_g/U_{mf}). In (b), $x_{f(0)}$ is the run-out of nonfluidized flows ($U_g = 0$) and is corrected for the volume of material that is left behind in the reservoir for nonfluidized and aerated flows (see text for details). Error bars are smaller than the symbols. Note that bubbles form at $U_g/U_{mf} \approx 2$ for group A particles.

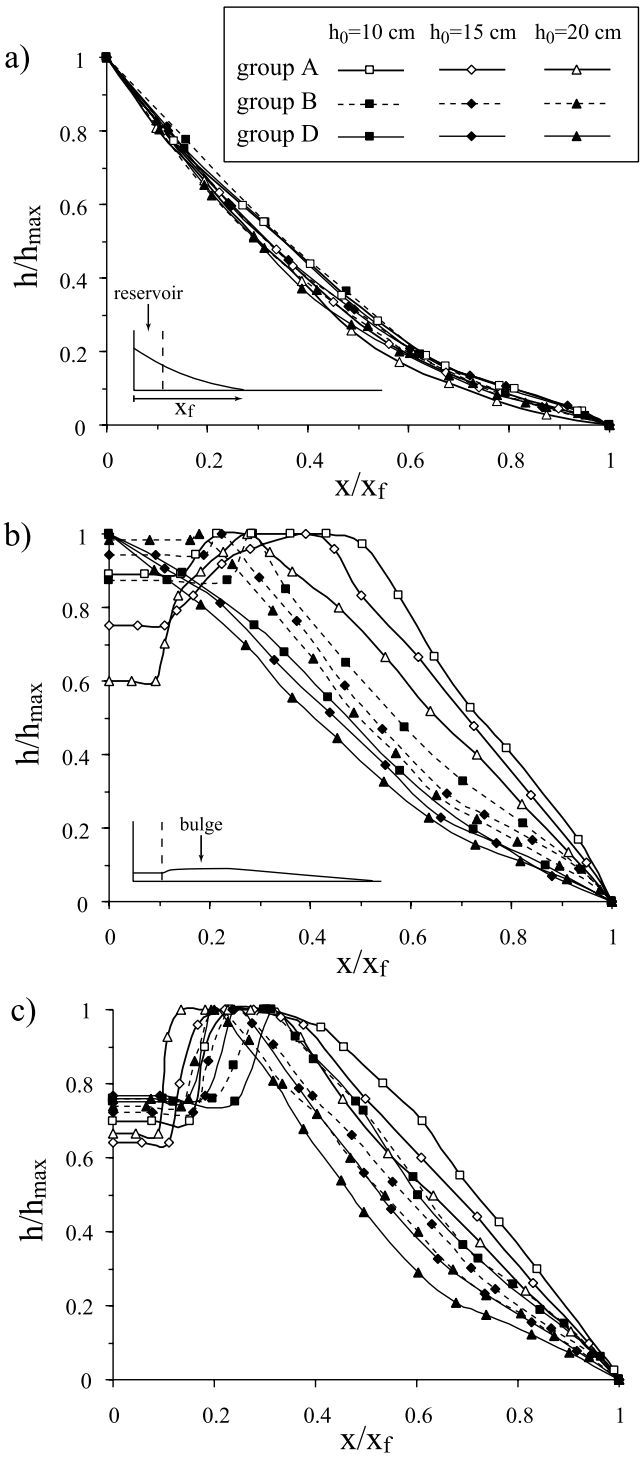

Figure 8. Height profiles of the deposits (h/h_{max}) as a function of the relative distance (x/x_f) for initial beds in the reservoir at (a) $U_g = 0$, (b) $U_g = U_{mf}$, and (c) $U_g = 2U_{mf}$. Inserts show the morphological characteristics of the deposits.

beds with nonfluidized beds of the same volume of actively flowing material. However, we find that corrections of x_f made in this way are of 1 cm to 4 cm and are only significant for flows of group D particles at $U_g/U_{mf} < 1$.

[18] In Figure 7b, the corrected data collapse for group B and D particles for initial bed heights of 10–20 cm, which shows that the run-out distance of initially fluidized flows is proportional to that of their nonfluidized counterparts. This run-out distance increases by a maximum factor of ≈1.8 and ≈1.3 for group B and D particles, respectively. In contrast, the data do not collapse for group A particles; the relative increase in flow run-out increases with the initial bed height. The maximum relative increase is of a factor of ≈1.95–2.2 for incipiently fluidized beds at $U_g/U_{mf} = 1.25$.

4.4. Deposit Characteristics

[19] The height profiles of the deposits differ, depending on the initial fluidization state (Figure 8). For nonfluidized flows (Figure 8a), the maximum height of the deposit (h_{max}) is at the backwall of the reservoir where the slope is equal to or slightly smaller than the angle of repose of the material. Deposit geometries are nearly similar as the height profiles do not depend on the grain size, but h/h_{max} slightly increases at a given relative distance x/x_f as the initial bed height h_0 decreases. For incipiently fluidized beds (Figure 8b), deposits of flows of the different groups of particles are clearly distinguishable. Deposits of group A and B particles are horizontal in the reservoir, and h_{max} is located further downflow. This results in a proximal bulge, commonly with a flat, horizontal surface. An upstream slope of 1°–2° is observed in some cases. The bulge may represent more than half the length of the deposit for group A particles. At a given relative distance, h/h_{max} increases as h_0 and the grain size decrease. In contrast, deposits of group D particles are similar in shape to the nonfluidized cases. At higher degrees of initial fluidization (Figure 8c), the height profiles for group B and D particles become more similar to those of group A particles. The height profile of group A particles does not change much with the degree of initial fluidization compared to an incipiently fluidized bed (Figure 8b). All deposits exhibit a bulge of constant height.

5. Interpretation of the Results

5.1. Flow Emplacement

[20] Initially fluidized flows of group A particles propagate at near constant velocity and thickness for much of their emplacement and have a relatively long run-out. In contrast, all other flows propagate as a wedge without any period of constant velocity and show shorter run-out distances. We now discuss some possible mechanisms to explain these two flow styles.

[21] As the flow run-out distance scales approximately with the initial pressure drop across the bed for a constant initial height h_0 (Figure 7), this may suggest that, other things being equal, a pore pressure diffusion timescale could determine the flow emplacement style as high pore pressure will reduce internal friction of a granular flow [*Denlinger and Iverson*, 2001]. A detailed analysis is beyond the scope of the paper and the aim here is rather to estimate orders of magnitude of pore pressure diffusion timescales. The pore pressure diffusion timescale is $t_{dif} = h_f^2/D$, where h_f is the flow thickness and D is the pore pressure diffusivity [*Iverson and LaHusen*, 1989], given by $D = k/(\varepsilon\mu_g\beta_g)$, where k is the bed permeability and β_g is the gas compressibility [*Liang et al.*, 2001]. In our experiments, calculations

are not straightforward as h_f varies with time in some cases. However, estimates indicate that t_{dif} is only $\approx 10^{-2}$–10^{-5} s for group B and D particles and so at least 2 orders of magnitude smaller than the flow duration ($\approx$1 s), whereas t_{dif} approaches 10^{-1} s for larger flows of group A particles, still an order of magnitude less than the flow duration. This shows that initial pore pressure is likely to be immediately diffused in flows of group B and D particles, whereas a significant pore pressure might be sustained in the early stages of propagation of group A particles.

[22] The flow characteristics could alternatively be determined by a deaeration timescale t_{de} related to the collapse of initially expanded flows. This can be calculated for initially fluidized flows of group A particles which propagate at constant thickness, taking into account their initial expansion and the deaeration rate, U_{de}. The deaeration timescale increases with bed depth and this may explain the increased mobility of initially deeper beds (Figure 7). However, the maximum t_{de} is only $\approx$35–55% of the duration of the flow. Furthermore, deaeration cannot be invoked for initially nonexpanded or slightly expanded fluidized flows ($U_g/U_{mf} \sim 1$), which have run-outs larger than that of fully expanded flows (Figure 7). For group B and D particles, very small initial dense phase expansion and high deaeration rate cause immediate collapse of the bed. The run-out of the initially fluidized flows scales with the bulk bed expansion, which provides additional potential energy to convert into a higher kinetic energy (Figures 3 and 7). These observations suggest that the flow characteristics can only partially be interpreted by simple deaeration of an initially expanded bed.

[23] The effect of passing gas through the initial bed will be to change the distribution of interparticle forces within it. In a static granular bed, the gravitational forces are transmitted to the boundaries through the agency of friction along a network of contact chains [*Jaeger et al.*, 1996]. On a scale of a few grains, local forces can be larger than the macroscale hydrostatic bed weight and chains surround regions where forces are smaller. The drag exerted by the gas flow on the particles will reduce their effective weight, and hence reduce the frictional forces within the bed. When the particles are fully fluidized, if the flow is homogeneous, then the force chains may become transient, or even be eliminated and therefore the bed of particles will become mobile. Disruption of the contact network caused by agitation of the particles and dilation of the flow results in the dense granular medium displaying a fluid-like behavior [*G. D. R. Midi*, 2004]. Once the current is moving the motion will cause dilation and the force chain network will continue to be disrupted until the flow decelerates and stops.

[24] Nonfluidized beds are in a solid-like state in that there is significant internal friction and they can then possess a yield stress, and this may explain why their initial acceleration is slower in comparison to initially fluidized beds of group A and B (cf. section 4.2). In contrast initially fluidized flows of group D particles behave nearly the same as their nonfluidized counterparts. A cause of this might be the heterogeneous nature of flow through group D particles: In beds of large particles, though they are fluidized in an overall sense, there is very vigorous motion near the bubbles while the particles between the bubbles are almost static [*Rahman and Campbell*, 2002]. Therefore significant parts of the bed may not be fully fluidized, and the force chains may persist there. This is in contrast to beds of group A particles where the bubbles do not exist, or are small, and the flow through bed is macroscopically homogeneous. In this case, the particles will be fluidized throughout the bed and there will be no persistent force chains or no chains at all, permitting greater mobility. In the aerated case at $0 < U_g < U_{mf}$, static contact forces are lowered by the fluid drag resulting in a decrease of the angle of repose [*Eames and Gilbertson*, 2000]. The geometry of the force chain network may also be modified by redistribution of intergrain contacts. As the gas flow rate increases, the intensity of forces in individual chains and possibly the number of chains decreases until the fluidized state is reached and this would explain the higher acceleration compared to the nonfluidized state. Subsequent slumping, and energy derived by motion maintains the system in a fluid-like state, and this may explain the high lateral acceleration (close to 1 g in some cases) as well as the higher speed and longer run-out.

[25] The dynamics of the flows are inferred to be determined by two regimes, according to variation in the flow friction due to agitation of the particles and dilation [*G. D. R. Midi*, 2004]. The first regime exists before onset of strong interparticle contacts (in the case where these were initially disrupted) with internal friction being negligible. The second subsequent regime develops when internal friction is nonnegligible because of significant interparticle contacts, but the chains have a short lifetime and are continuously regenerated. For initially aerated flows, which may enter the second regime directly, the longer flow run-out as the degree of fluidization increases may be caused by decreasing intensity and number of interparticle contacts compared to the nonfluidized state. Flow emplacement and run-out distances suggest contrasting timescales of the two regimes for initially fluidized flows of fine group A particles and coarser particles (Figures 4 and 7). The timescale of the first, negligible friction regime (i.e., before the onset of strong contacts) represents most of the flow duration for group A particles whereas it is much reduced for groups B and D particles. Initially fluidized flows of group A particles propagate with a horizontal upper surface and this suggests very low intergrain contacts and internal friction for most of their duration. Above the condition of minimum fluidization, the contact network is significantly disrupted and weakened. Initial bed expansion has little influence on the flow emplacement (Figures 6 and 7). Similar flow velocities and run-outs for different initial bed expansions suggest that the deaeration is not the controlling process. In contrast, the timescale of the second, nonnegligible internal friction regime when strong contacts are reestablished is small for group A particles, whereas it represents most, if not all, the flow duration for group B and D particles.

[26] When the flow finally declines in energy due a rapid increase in internal friction and ceases motion, a third regime determines the time needed for the final contacts chain network to rebuild, and we call this regime the "stopping phase" of the flow. Shearing within the slow flow leads to an increase in the strength of the chain network [*Hartley and Behringer*, 2003], which in turn would act as a positive feedback effect to stop the flow motion. This may be interpreted as a "phase change" and the timescale of the final stage of emplacement is a measure

of the kinetics required to convert the granular medium from the fluid-like state back to the solid-like, static state.

[27] Our experiments show a gradual change in flow characteristics as a function of the grain size of the particles. However, initially fluidized flows of group A and B particles show distinct behavior, even although the difference in grain size is small, which suggests a distinct break for the behavior of flows of particles of these groups (Figure 7). The experiments of *Lube et al.* [2004] on axisymmetric release of granular columns have defined two flow regimes for flows of coarse particles ($d_p > 300$ μm, groups B and D), depending on the initial bed aspect ratio (bed height/half reservoir diameter). Flows generated from beds at aspect ratios smaller than 1.7 propagate at a decelerating velocity after an initial acceleration of ≈0.25–0.3 g, as seen in our experiments. However for beds at aspect ratios larger than 1.7, flows propagate at constant velocity. Our 2-D experiments carried out at equivalent bed aspect ratios of 1 to 2 show that a constant flow velocity regime can nevertheless develop provided the bed is initially fluidized and the particles are sufficiently small (group A). Alternatively in our system, a constant flow velocity might be observed for beds of group B and D particles at aspect ratios significantly larger than 1.7. *Lube et al.* [2004] observed that flows enter a final stopping phase of emplacement whose timescale is constant. As flow duration increases with the initial bed height, the relative duration of the stopping phase decreases and may represent as little as ≈5% of the flow duration.

5.2. Flow Dynamics

[28] The fluid analogs to our collapsing granular flow experiments are lock exchange and the dam break experiments [*Benjamin*, 1968; *Simpson*, 1997]. These experiments consist of release of a gravity current with the denser (current) fluid initially in a lock and the lighter (ambient) fluid in a channel. Lock exchange experiments refer to a small density difference between the current and the ambient medium, known as the Boussinesq condition [*Huppert and Simpson*, 1980; *Rottman and Simpson*, 1983]. Dam break experiments refer to the condition of large density contrast between the fluids as in our experiments [*Benjamin*, 1968; *Gröbelbauer et al.*, 1993]. We show here that the granular flows we have studied reveal some of the characteristics of both systems.

[29] In lock exchange experiments, on removal of the lock gate separating the fluids, the denser fluid collapses under gravity and flows out of the lock, generating a counter current of light fluid. The propagation of the dense fluid along the channel takes place in three regimes [*Huppert and Simpson*, 1980; *Rottman and Simpson*, 1983]. After initial acceleration, there is an initial slumping regime during which the gravity current front velocity is constant and the motion is affected by interaction with the counter flow, but whose effect decreases as the ratio of the flow thickness over the depth of the ambient medium decreases. This is followed by an inertia-buoyancy regime in which the inertial and buoyancy forces at the current front are in balance. The current thickness steadily decreases with time and the front position increases as the 2/3 power of time. Finally, there is a viscous regime in which the viscous and buoyancy forces are in balance and the front position increases as the 1/5 power of time. During the slumping regime the flow is controlled by a Froude number condition at its front, $Fr = U_f/(g'h_f)^{1/2}$, where U_f is the front velocity, h_f is the height of the current and g' is the reduced gravity, defined as $g' = g(\Delta\rho/\rho_{ref})$. The ρ_{ref} is conventionally taken as the density of the less dense fluid, but its definition does not matter for the Boussinesq limit for which the condition $g' < g$ is fulfilled [*Benjamin*, 1968]. The Froude number condition was also studied for the dam break case where ρ_{ref} is taken as the density of the dense fluid so that g' approaches g but is smaller (see *Gröbelbauer et al.* [1993] for discussion). In our case, $g' \sim g$ so that

$$Fr = \frac{U_f}{(gh_f)^{1/2}}. \tag{3}$$

The granular flows described in this paper can be compared with both types of fluid gravity currents in terms of the flow regimes, height and shape of the current, and Froude number.

[30] In lock exchange experiments, dimensional analysis have been used to define two length and timescales; $x^* = (x - x_0)/x_0$ and $t^* = t/t_0$, where x_0 is the lock length, $t_0 = x_0/(g'h_0)^{1/2}$, and h_0 is the depth of dense fluid in the lock prior to opening [*Rottman and Simpson*, 1983]. Experimental data scaled in this form collapse to straight lines when $x^* = f(t^*)$ is plotted on logarithmic axes, with slopes of 1 (slumping regime), 2/3 (inertial-buoyancy regime) and 1/5 (viscous regime). We have plotted similar graphs for our experiments (data in Figure 5), for which the initial acceleration phase is taken into account but is not represented (Figure 9). There is a good collapse of the data for different initial bed heights (as from *Rottman and Simpson* [1983]) for the same grain size and under the same initial fluidization conditions. Two distinct regimes appear for each experiment: After the initial acceleration phase (not shown), the data fit a straight line; a break then occurs for the last 4–6 data points before the flow ceases motion and we define this as the stopping phase. For initially fluidized flows of group A particles, the data collapse along a straight line with a slope of 0.96, very close to the theoretical value of 1 for constant flow velocity. During this nearly constant velocity regime, the flow thickness is constant while the flow is fed from the reservoir. Subsequently, the flow can propagate by the spreading of its frontal part, and the front velocity remains constant for a while. Compared to fluid gravity currents produced in lock exchange experiments, these granular flows do not enter a regime where the front position increases as the 2/3 power of time. This may be because the granular flow thickness does not progressively decrease with time, as in currents of simple fluids, because flows propagate at almost the same density as the final deposit and rapidly freeze. In contrast, the data for all other flows fit slopes of ≈0.80, suggesting the same flow dynamics and deceleration for different experiments. At a given time after release, initially fluidized flows of group B and D particles have propagated further than nonfluidized flows, but the difference reduces as the grain size increases. This may be explained by a faster acceleration for initially fluidized flows compared to their nonfluidized counterparts as the grain size decreases, as discussed in section 4.2. A rapid return to a state similar to that of a nonfluidized flow may explain similar power law behavior in the deceleration

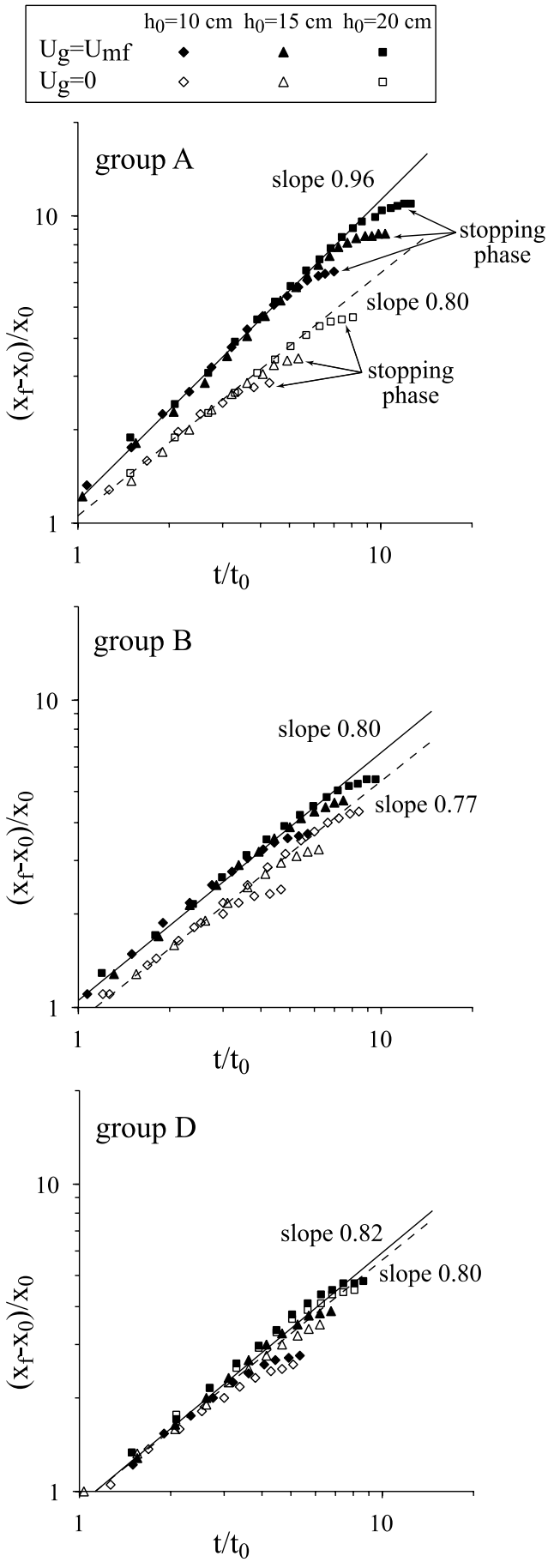

phase. We propose that this is similar to the slumping regime of fluid gravity currents (power of 1), but in these cases significant interparticle contacts remain or are reestablished, thus promoting nonnegligible internal flow friction. For all flows in their final stages, the data depart significantly from the power laws with rapid deceleration and an abrupt stop, and the data fit slopes of ≈0.3–0.4 (not shown in Figure 9). This is the stopping phase of the flow, whose timescale is ≈0.2 s, and closely matches the results of *Lube et al.* [2004], suggesting a similar "stopping mechanism" operating independently of the degree of initial fluidization, bed height, and grain size.

[31] Under dam break conditions, fluid gravity currents have a constant thickness along their length as mixing with the ambient fluid at the front is limited, and the current front has a slope to the horizontal $\Theta = 60°$ [*Benjamin*, 1968; *Gröbelbauer et al.*, 1993]. In our experiments, initially fluidized flows of particles of group A can be compared with these fluid currents as they also propagate at constant thickness and frontal velocity. At early stages of propagation $\Theta \approx 50°–60°$ (Figures 4 and 10). The flow depth (h_f) scaled on initial bed height (h_0) has the value of ≈0.2, compared with the theoretical value of 0.25 calculated by *Fanneløp and Waldman* [1972], however, that was for Boussinesq gravity currents (Figure 10). We determined a Froude number by plotting the front velocity U_f as a function of $(gh_f)^{1/2}$ according to equation (3) (Figure 11). For experiments at various initial conditions, the data fall along a straight line whose slope is $Fr = 2.58$. The degree of initial fluidization has no systematic influence on h_f and U_f. By making a comparison with the data of *Gröbelbauer et al.* [1993], we find that $Fr = 2.58$ is in good agreement with the value determined in their experiments and close to the theoretical prediction for dam breaking ($Fr = 2\sqrt{2}$, Figure 12).

5.3. Implications for Pyroclastic Flows Emplacement

[32] Pyroclastic flows commonly contain large amounts of fine ash [*Sparks*, 1976] and particles of group A are likely to represent up to >50–60% in some cases. A characteristic of pyroclastic flows is their high mobility and our experiments on dense mixtures showed that initially fluidized flows can run out to about twice the distance of their nonfluidized counterparts. Emplacement in a fluidized state may then explain the sheet-like character of many pyroclastic deposits having an upper slope of only a few degrees [*Hildreth*, 1983; *Hoblitt*, 1986; *Wilson et al.*, 1995; *Calder et al.*, 2000; *Cole et al.*, 2002]. According to our results, we infer that dense, fines-rich pyroclastic flows can

Figure 9. Nondimensional kinematic data showing the flow front position from the reservoir gate ($x_f - x_0$), as a function of time with $t_0 = x_0/(gh_0)^{1/2}$ according to *Rottman and Simpson* [1983], where h_0 is the initial bed height. Data are for flows generated from nonfluidized ($U_g = 0$) and incipiently fluidized beds ($U_g = U_{mf}$). Best fits ($R^2 = 0.98–0.99$) neglect data of the initial acceleration phase (not represented) and of the final stopping phase (last 4–6 data points chosen arbitrarily). They give slopes of ≈0.8 except for initially fluidized flows of group A particles for which the slope is ≈1 (constant velocity).

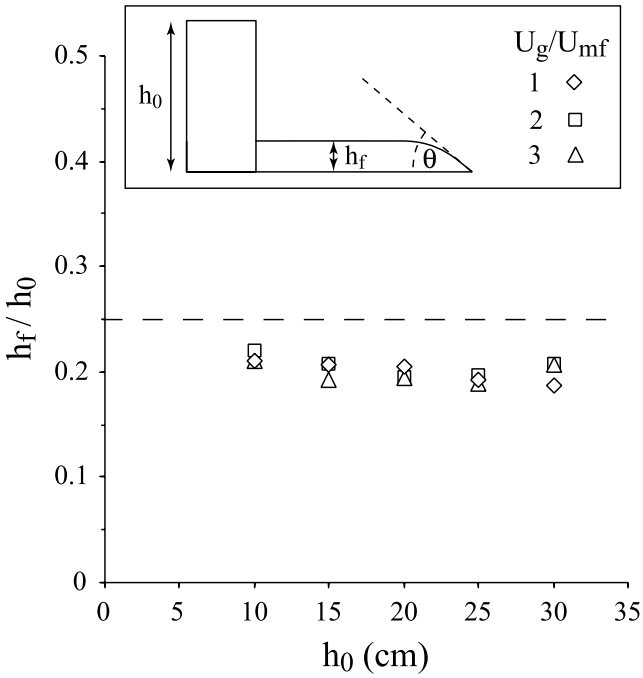

Figure 10. Flow thickness (h_f) over initial bed height (h_0) for initially fluidized flows of group A particles. The slope of the flow front (Θ) at early stages of propagation is ≈50°–60°. Slight variations of 1–2 mm for h_f are observed during flow propagation but variations of calculated values are smaller than the size of the symbols. The horizontal dashed line is the theoretical prediction for Boussinesq fluid gravity currents [*Fanneløp and Waldman*, 1972].

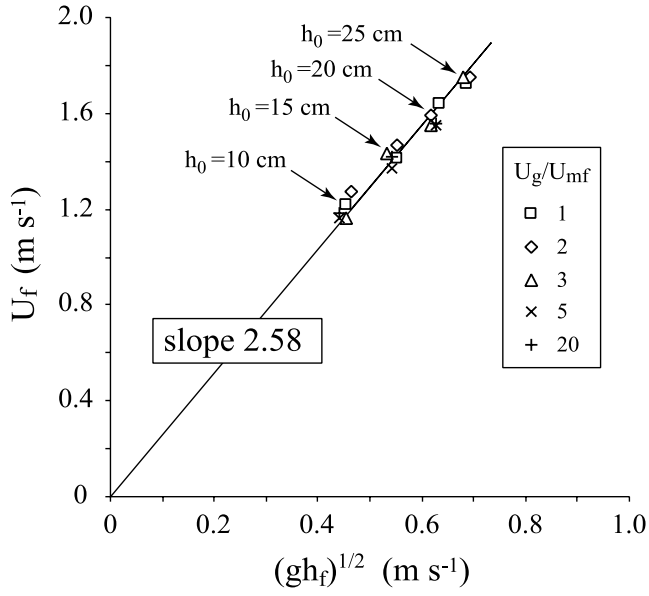

Figure 11. Froude number $Fr = U_f/(gh_f)^{1/2}$ (equation (3)) for flows of particles of group A at various initial degrees of fluidization (U_g/U_{mf}) and bed heights (h_0). The flow front velocity (U_f) is obtained from fits of data from the constant-velocity phase (Figure 5). Variations due to uncertainties of the flow thickness (h_f) are smaller than the size of the symbols. The best fit gives Fr = 2.58 (R^2 = 0.97).

be described, except at the very final stages of emplacement, as inviscid fluid gravity currents. Ignoring possible early stages of emplacement at high velocity due to generation by column collapse and assuming flow propagation at quasiequilibrium under gravity, this predicts (using a Froude number of 2.6) a velocity of 8–26 m s^{-1} for flow thicknesses of 1–10 m, which is consistent with observations of pyroclastic flows propagating on slopes of a few degrees [*Hoblitt*, 1986; *Cole et al.*, 2002; *Druitt et al.*, 2002; *Loughlin et al.*, 2002]. Flows thicker than 100 m may have speeds higher than 80 m s^{-1}, but flow compressibility might complicate this simple picture.

[33] *Levine and Kieffer* [1991] successfully reproduced the observed velocities of the 7 August 1980, pyroclastic flows at Mount St. Helens [*Hoblitt*, 1986] using open-channel hydraulic theory for flow of an inviscid fluid down a channel. In areas where there were no rapid channel geometry changes likely to influence the flow propagation strongly, they calculated a Froude number of 2.4–2.8 [*Levine and Kieffer*, 1991, Table 1]. Although there are probably many significant differences in the physics of a pyroclastic flow compared with a fluid channel flow, it does provide some support for the importance of flow processes, such as that we propose, to pyroclastic flows.

[34] An important aspect of this study is that the choice of a relevant Froude number is important for appropriate flow modeling, and the density contrast between the flow and the ambient medium is a fundamental parameter. This issue has recently been investigated by *Nield and Woods* [2004]. For instance, Froude numbers of ≈1, as typically obtained in experiments carried out under Boussinesq conditions, lead to underestimates of the frontal velocity of a flow of a given height. Our study could also apply to other types of dense

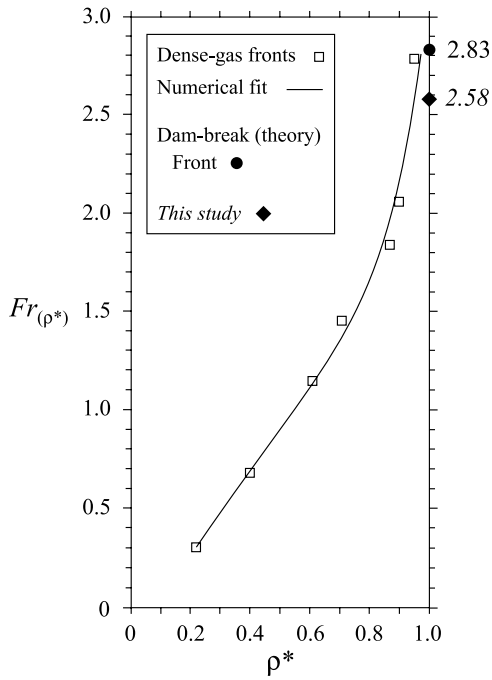

Figure 12. Froude number $Fr_{(\rho^*)} = U_f/(gh_f)^{1/2}$ as a function of $\rho^* = [(\rho_{dense} - \rho_{light})/(\rho_{dense} + \rho_{light})]^{1/2}$ for fluid gravity currents and our experimental flows with particles of group A propagating in an infinite ambient medium; see text for details. Modified after *Gröbelbauer et al.* [1993].

geophysical flows. For example some snow avalanches might also exhibit the fluid-like behavior revealed in our experiments due to air ingestion at the flow front [*Hopfinger*, 1983]. More generally, flows generated from agitation and dilation of a fast moving granular flow or sedimentation from a dilute, expanded mixture may share similar dynamical behavior.

6. Conclusions

[35] Our small-scale laboratory granular flows under conditions of initial aeration and fluidization provides insights into the dynamics of granular flow systems generally. We interpret the experimental results in terms of the intensity of intergranular contacts that strongly influence the internal friction. These basically depend on the initial bed conditions, such as the average strength of the force chain network, on flow motion generating dilation and on the timescale required for reestablishment of strong frictional particle contacts. The experiments have revealed two contrasting patterns of behavior after initial acceleration, for initially fluidized flows of group A particles and other types of flows respectively.

[36] Initially fluidized, concentrated flows of fine particles of group A propagate at constant thickness and velocity for most of their duration, and are in a regime similar to the slumping regime of high Reynolds number gravity currents of Newtonian fluids. As the description of these simple currents neglects viscosity (and thus internal friction) this suggests that internal particle friction can also be neglected in our flows. These granular flows have a morphology similar to their fluid analogs, as shown by the shape of the head and the ratio h_f/h_0, and we have determined a Froude number $Fr \approx 2.6$, which is consistent with published data from experimental and theoretical investigations of slumping gravity currents of Newtonian fluids. Initial fluidization of the bed reduces the effects of intergranular contacts, and renders the bed into a mobile, fluid-like state. Motion additionally generates mild dilation and some timescale is needed before onset of a nonnegligible internal friction regime when strong interparticle contacts are reestablished. Other granular flows propagate as a wedge with a decelerating velocity as their front position increases as the $\sim$0.8 power of time, because of significant interparticle contacts, promoting nonnegligible internal flow friction. Rapid transition to a nonnegligible frictional regime is favored by an initial nonfluidized state of the bed, and by large grain size. The rebuilding of contact chains might be manifested in significant basal sedimentation during emplacement, which reduces the flowing ability and promotes flow deceleration. All flows eventually enter a final stopping phase of emplacement when they decline in energy due a rapid increase in internal friction and cease motion. The timescale of this stopping phase ($\approx$0.2 s) gives an estimate of the kinetics required for a 'phase change' to convert the granular material from the fluid-like state back to the solid-like, static state.

[37] We infer that fines-rich pyroclastic flows may propagate as initially fluidized flows of group A particles, which are like gravity currents of Newtonian fluids for most of their duration. In this context, flow velocities calculated with $Fr = 2.6$ obtained in our experiments are consistent with that determined from field observations of pyroclastic flows propagating on gentle slopes. Further investigations are needed to better characterize how the timescales before onset of strong interparticle contacts and before onset of the stopping phase vary as a function of the grain size of the particles, and to determine the influence of the slope angle and of grain size distribution on flow mechanisms.

[38] **Acknowledgments.** O. R. was supported by a EC Marie Curie Fellowship while at Bristol University, and R. S. J. S. by a NERC Professorship. Frames were captured using the UTHSCSA ImageTool program developed at the University of Texas Health Science Center, San Antonio (anonymous FTP, maxrad6.uthscsa.edu). The paper benefited from stimulating discussions with Tim Druitt and Andrew Hogg, and thorough reviews by Roger Denlinger, Colin Wilson, and an anonymous Associate Editor.

References

Benjamin, T. B. (1968), Gravity currents and related phenomena, *J. Fluid Mech.*, *31*, 209–248.

Branney, M. J., and P. Kokelaar (2002), *Pyroclastic Density Currents and the Sedimentation of Ignimbrites*, *Mem. Geol. Soc. London*, *27*, 152 pp.

Calder, E. S., R. S. J. Sparks, and M. C. Gardeweg (2000), Erosion, transport and segregation of pumice and lithic clasts in pyroclastic flows inferred from ignimbrite at Lascar Volcano, Chile, *J. Volcanol. Geotherm. Res.*, *104*, 201–235.

Campbell, C. S. (1990), Rapid granular flows, *Annu. Rev. Fluid Mech.*, *22*, 57–92.

Cole, P. D., E. S. Calder, R. S. J. Sparks, A. B. Clarke, T. H. Druitt, S. R. Young, R. A. Herd, C. L. Harford, and G. E. Norton (2002), Deposits from dome-collapse and fountain-collapse pyroclastic flows at Soufrière Hills Volcano, Montserrat, in *The Eruption of Soufrière Hills Volcano, Montserrat, From 1995 to 1999*, edited by T. H. Druitt and B. P. Kokelaar, *Mem. Geol. Soc. London*, *21*, 231–262.

Denlinger, R. P., and R. M. Iverson (2001), Flow of variably fluidized granular masses across three-dimensional terrain: 2. Numerical predictions and experimental tests, *J. Geophys. Res.*, *106*, 553–566.

Druitt, T. H. (1998), Pyroclastic density currents, in *The Physics of Explosive Volcanic Eruptions*, edited by J. S. Gilbert and R. S. J. Sparks, *Geol. Soc. Spec. Publ.*, *145*, 145–182.

Druitt, T. H., E. S. Calder, P. D. Cole, R. P. Hoblitt, S. C. Loughlin, G. E. Norton, L. J. Ritchie, R. S. J. Sparks, and B. Voight (2002), Small-volume, highly mobile pyroclastic flows formed by rapid sedimentation from pyroclastic surges at Soufrière Hills Volcano, Montserrat: An important volcanic hazard, in *The Eruption of Soufrière Hills Volcano, Montserrat, From 1995 to 1999*, edited by T. H. Druitt and B. P. Kokelaar, *Mem. Geol. Soc. London*, *21*, 263–279.

Eames, I., and M. A. Gilbertson (2000), Aerated granular flow over a horizontal rigid surface, *J. Fluid Mech.*, *424*, 169–195.

Fanneløp, T. K., and G. D. Waldman (1972), Dynamics of oil slicks, *AIAA J.*, *10*, 506–510.

Geldart, D. (1973), Types of gas fluidization, *Powder Technol.*, *7*, 285–292.

Geldart, D., and A. C. Y. Wong (1985), Fluidization of powders showing degrees of cohesiveness, II, Experiments on rates of deaeration, *Chem. Eng. Sci.*, *40*, 653–661.

Gilbertson, M., and I. Eames (2003), The influence of particle size on the flow of fluidized powders, *Powder Technol.*, *131*, 197–205.

Goldhirsch, I. (2003), Rapid granular flows, *Annu. Rev. Fluid Mech.*, *35*, 267–293.

Gröbelbauer, H. P., T. K. Fanneløp, and R. E. Britter (1993), The propagation of intrusion fronts of high density ratios, *J. Fluid Mech.*, *250*, 669–687.

Groupement de Recherche Milieux Divisés (G. D. R. Midi) (2004), On dense granular flows, *Eur. Phys. J. E*, *14*, 341–365.

Hartley, R. R., and R. P. Behringer (2003), Logarithmic rate dependence of force networks in sheared granular materials, *Nature*, *421*, 928–931.

Hildreth, W. (1983), The compositionally zoned eruption of 1912 in the Valley of Ten Thousand Smokes, Katmai National Park, Alaska, *J. Volcanol. Geotherm. Res.*, *18*, 1–56.

Hoblitt, R. P. (1986), Observations of the eruptions of July 22 and August 7, 1980, at Mount St. Helens, Washington, *U.S. Geol. Surv. Prof. Pap.*, *1334*, 44 pp.

Hopfinger, E. J. (1983), Snow avalanche motion and related phenomena, *Annu. Rev. Fluid Mech.*, *15*, 47–76.

Huppert, H. E., and J. E. Simpson (1980), The slumping of gravity currents, *J. Fluid Mech.*, *99*, 785–799.

Ishida, M., H. Hatano, and T. Shirai (1980), The flow of solid particles in an aerated inclined channel, *Powder Technol.*, *27*, 7–12.

Iverson, R. M., and R. G. LaHusen (1989), Dynamic pore-pressure fluctuations in rapidly shearing granular materials, *Science*, *246*, 796–799.

Jaeger, H. M., S. R. Nagel, and R. P. Behringer (1996), Granular solids, liquids, and gases, *Rev. Modern Phys.*, *68*, 1259–1273.

Johnson, P. C., and R. Jackson (1987), Frictional-collisional constitutive relations for granular materials, with application to plane shearing, *J. Fluid Mech.*, *176*, 67–93.

Johnson, P. C., P. Nott, and R. Jackson (1990), Frictional-collisional constitutive relations for granular materials, with application to plane shearing, *J. Fluid Mech.*, *210*, 501–535.

Levine, A. H., and S. W. Kieffer (1991), Hydraulics of the August 7, 1980, pyroclastic flow at Mount St. Helens, Washington, *Geology*, *19*, 1121–1124.

Liang, Y., J. D. Price, D. A. Wark, and E. B. Watson (2001), Nonlinear pressure diffusion in a porous medium: Approximate solutions with applications to permeability measurements using transient pulse decay method, *J. Geophys. Res.*, *106*, 529–535.

Loughlin, S. C., E. S. Calder, A. Clarke, P. D. Cole, R. Luckett, M. T. Mangan, D. M. Pyle, R. S. J. Sparks, B. Voight, and R. B. Watts (2002), Pyroclastic flows and surges generated by the 25 June 1997 dome collapse, Soufrière Hills Volcano, Montserrat, in *The Eruption of Soufrière Hills Volcano, Montserrat, From 1995 to 1999*, edited by T. H. Druitt and B. P. Kokelaar, *Mem. Geol. Soc. London*, *21*, 191–209.

Lube, G., H. E. Huppert, R. S. J. Sparks, and M. A. Hallworth (2004), Axisymmetric collapses of granular columns, *J. Fluid Mech.*, *508*, 175–199.

Mangeney-Castelnau, A., J.-P. Vilotte, M. O. Bristeau, B. Perthame, F. Bouchut, C. Simeoni, and S. Yernini (2003), Numerical modeling of avalanches based on Saint-Venant equations using a kinetic scheme, *J. Geophys. Res.*, *108*(B11), 2527, doi:10.1029/2002JB002024.

Nield, S. E., and A. W. Woods (2004), Effects of flow density on the dynamics of dilute pyroclastic density currents, *J. Volcanol. Geotherm. Res.*, *132*, 269–281.

Nott, P., and R. Jackson (1992), Frictional-collisional equations of motion for granular materials and their applications to flow in aerated chutes, *J. Fluid Mech.*, *241*, 144–145.

Pouliquen, O. (1999a), Scaling laws in granular flows down rough inclined planes, *Phys. Fluids*, *11*, 542–548.

Pouliquen, O. (1999b), On the shape of granular fronts down rough inclined planes, *Phys. Fluids*, *11*, 1956–1958.

Rahman, K., and C. S. Campbell (2002), Particle pressures generated around bubbles in gas-fluidized beds, *J. Fluid Mech.*, *455*, 103–127.

Rhodes, M. J. (1998), *Introduction to Particle Technology*, John Wiley, Hoboken, N. J.

Roche, O., M. Gilbertson, J. C. Phillips, and R. S. J. Sparks (2002), Experiments on deaerating granular flows and implications for pyroclastic flow mobility, *Geophys. Res. Lett.*, *29*(16), 1792, doi:10.1029/2002GL014819.

Rottman, J. W., and J. E. Simpson (1983), Gravity currents produced by instantaneous releases of a heavy fluid in a rectangular channel, *J. Fluid Mech.*, *135*, 95–110.

Savage, S. B. (1984), The mechanics of rapid granular flows, *Adv. Appl. Mech.*, *24*, 289–366.

Savage, S. B., and K. Hutter (1989), The motion of a finite mass of granular material down a rough incline, *J. Fluid Mech.*, *199*, 177–215.

Simpson, J. E. (1997), *Gravity Currents in the Environment and the Laboratory*, 2nd ed., Cambridge Univ. Press, New York.

Sparks, R. S. J. (1976), Grain size variations in ignimbrites and implications for the transport of pyroclastic flows, *Sedimentology*, *23*, 147–188.

Sparks, R. S. J. (1978), Gas release rates from pyroclastic flows: An assessment of the role of fluidisation in their emplacement, *Bull. Volcanol.*, *41*, 1–9.

Takahashi, T., and H. Tsujimoto (2000), A mechanical model for Merapi-type pyroclastic flow, *J. Volcanol. Geotherm. Res.*, *98*, 91–115.

Wilson, C. J. N. (1980), The role of fluidization in the emplacement of pyroclastic flows: An experimental approach, *J. Volcanol. Geotherm. Res.*, *8*, 231–249.

Wilson, C. J. N. (1984), The role of fluidization in the emplacement of pyroclastic flows, 2, Experimental results and their interpretation, *J. Volcanol. Geotherm. Res.*, *20*, 55–84.

Wilson, C. J. N., B. F. Houghton, P. J. J. Kamp, and M. O. McWilliams (1995), An exceptionally widespread ignimbrite with implications for pyroclastic flow emplacement, *Nature*, *378*, 605–607.

M. A. Gilbertson, Department of Mechanical Engineering, Centre for Environmental and Geophysical Flows, University of Bristol, University Walk, Queen's Building, Bristol BS8 1TR, UK. (m.gilbertson@bristol.ac.uk)

J. C. Phillips and R. S. J. Sparks, Department of Earth Sciences, Center for Environmental and Geophysical Flows, University of Bristol, Queen's Road, Wills Memorial Building, Bristol BS8 1RJ, UK. (j.c.phillips@bristol.ac.uk; steve.sparks@bristol.ac.uk)

O. Roche, UMR Magmas et Volcans, Institut de Recherche pour le Développement, Université Blaise Pascal, 5 rue Kessler, F-63038 Clermont-Ferrand, France. (o.roche@opgc.univ-bpclermont.fr)